ADVANCED FUNCTIONAL MATERIALS
www.afm-journal.de

A Unified Picture of Aggregate Formation in a Model Polymer Semiconductor during Solution Processing

Fabian Panzer, Matthew J Dyson, Hazem Bakr, Stefan Wedler, Konstantin Schötz, Mihirsinh Chauhan, Paul N Stavrinou, Anna Köhler,* and Natalie Stingelin**

One grand challenge for printed organic electronics is the development of a knowledge platform that describes how polymer semiconductors assemble from solution, which requires a unified picture of the complex interplay of polymer solubility, mass transport, nucleation and, e.g., vitrification. One crucial aspect, thereby, is aggregate formation, i.e., the development of electronic coupling between adjacent chain segments. Here, it is shown that the critical aggregation temperatures in solution (no solvent evaporation allowed) and during film formation (solvent evaporation occurring) are excellent pointers to i) establish reliable criteria for polymer assembly into desired aggregates, and ii) advance mechanistic understanding of the overall polymer assembly. Indeed, important insights are provided on why aggregation occurs via a 1- or 2-step process depending on polymer solubility, deposition temperature and solvent evaporation rate; and the selection of deposition temperatures for specific scenarios (e.g., good vs bad solvent) is demystified. Collectively, it is demonstrated that relatively straightforward, concurrent in situ time-resolved absorbance and photoluminescence spectroscopies to monitor aggregate formation lead to highly useful and broadly applicable criteria for processing functional plastics. In turn, improved control over their properties and device performance can be obtained toward manufacturing sensors, energy-harvesting devices and, e.g., bioelectronics systems at high yield.

1. Introduction

The very local chain arrangement of polymer semiconductors is, in many cases, dictating the overall optoelectronic characteristics of this exciting and versatile class of materials because it determines whether adjacent chain segments ("chromophores") are electronically interacting, i.e., whether they form photophysical aggregates, or not.[1,2] Thereby, the nature and the quality of the induced aggregates play a decisive role in the material's optical behavior,[3–6] charge-transport properties,[7] and/or charge-separation capabilities, influencing device performance and efficiency.[5,8] For instance, for the ubiquitous poly(3-hexylthiophene) (P3HT), it was postulated that a balanced intra- versus inter-molecular excitonic coupling in higher quality aggregates leads to a high exciton coherence,[9] while excitons extrinsically dissociate between aggregates of different order/quality.[10] Vice versa, producing films comprised of homogenous

F. Panzer, H. Bakr, S. Wedler, K. Schötz, M. Chauhan, A. Köhler
Soft Matter Optoelectronics
University of Bayreuth
95440 Bayreuth, Germany
E-mail: fabian.panzer@uni-bayreuth.de; anna.koehler@uni-bayreuth.de

M. J Dyson
Molecular Materials and Nanosystems and Institute for Complex Molecular Systems
Eindhoven University of Technology
Eindhoven 5600 MB, The Netherlands

M. Chauhan
Department of Materials Science and Engineering and Organic and Carbon Electronics Laboratories (ORaCEL)
North Carolina State University
Raleigh, NC 27695, USA

P. N Stavrinou
Information Engineering Building, Department of Engineering Science
University of Oxford
Oxford OX1 3PJ, UK

N. Stingelin
School of Materials Science & Engineering and School of Chemical & Biomolecular Engineering
Georgia Institute of Technology
Atlanta, Georgia 30332, USA
E-mail: natalie.stingelin@gatech.edu

The ORCID identification number(s) for the author(s) of this article can be found under https://doi.org/10.1002/adfm.202314729

DOI: 10.1002/adfm.202314729

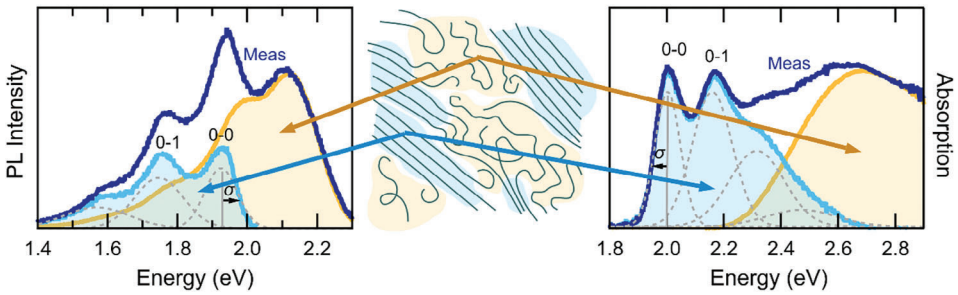

Figure 1. Absorption and photoluminescence spectra of P3HT in CF acquired during blade coating at $T_{substrate}$ = 5 °C, showing contributions from aggregated (light blue) and disordered, non-aggregated chains (orange). Subtracting the spectral contribution of the non-aggregated chains leaves a spectrum that can be attributed predominantly to the aggregated chains (light blue). The 0-0/0-1 peak ratio and peak width σ can be determined by fitting this extracted spectrum (dashed grey lines indicate individual vibronic peaks) using the models described in the discussion of **Figure 2**.

aggregate quality was shown to result in a narrow trap distribution and, hence, good transistor performance.[7]

The challenge to date has been that fine-tuning of aggregate quality and nature (see Ref.[5] for illustrative schematics) typically can only be achieved via time-consuming and elaborate trial-and-error procedures, especially when processing from solution.[1,11] Indeed, broadly applicable guidelines toward robust polymer semiconductor processing that allow reliable selection of processing parameters for targeted materials assembly are still missing. Here, we show on the prototypical semiconducting P3HT of a weight-averaged molecular weight M_w = 100 kg mol^{-1} that knowledge of the critical transition temperatures for aggregate formation both in solution (no solvent evaporation allowed) as well as during film formation when solvent is evaporating, permits gaining an understanding of the assembly process. This, in turn, enables the establishment of precise processing protocols for the creation of polymer semiconductor thin-film structures of desired properties. [A P3HT of M_w = 100 kg mol^{-1} was selected because, for concentrations typically used for device fabrication (10 mg ml^{-1}),[12] solutions are obtained that are above the critical concentration of entanglement, c_c, as shown in the Supporting Information.[2] This is important as higher quality aggregates can be introduced in films cast from solutions above c_c, while films produced with solutions comprising lower molecular weight materials (or very dilute systems) tend to result in aggregates of high torsional disorder.[2]]

2. Results and Discussion

To obtain initial information, we simultaneously recorded time-resolved in situ absorption and photoluminescence (PL) spectra of P3HT wet layers during blade coating at different deposition (substrate) temperatures and solvent quality, as well as of sealed solutions, and analyzed them with a modified Franck–Condon model. We selected for our study two solvents, chloroform (CF) and tetrahydrofuran (THF). The reason for this choice is that CF and THF have similar boiling temperatures (≈61 °C for CF; ≈66 °C for THF), but they display very different polarities, as can be deduced from their very different dielectric constants of 4.81 for CF and 7.58 for THF. Accordingly, P3HT displays a distinctly different solubility in the two solvents; P3HT is more soluble in CF than in THF —as also reflected by the Hansen solubility parameters presented in Table S1 (Supporting Information).[13]

To prepare for the discussion of our results, we start recalling how distinct signatures for aggregates (shaded in **Figure 1** in pale blue) and non-aggregated chromophores (pale orange) can be identified in the P3HT absorption and PL spectra. This is important because aggregated and disordered, non-interacting domains generally coexist in semiconducting polymer thin films; [1,2] hence, the measured optical spectra are a superposition of spectral signatures from both contributions. Thereby, we consider that the electronic coupling within the aggregates alters the spectral shape and reduces the energy of the aggregate spectra compared to non-aggregated chain segments.[14]

To extract the contribution of aggregates from the overall spectra in both absorbance and PL, we measured the spectra in solution at elevated temperatures where only non-aggregated material prevails (see Figure S1, Supporting Information). We then used the spectrum at the lowest possible temperature before aggregation sets in, normalized it to the high energy edge of the overall spectrum of a P3HT thin film, and subtracted it from the latter (Figure 1).[5] In both absorbance and PL, the resulting aggregate-only spectra exhibit a clear vibronic progression of the electronic $S_1 - S_0$ transition, with a peak spacing of 0.175 eV due to coupling with an effective vibrational mode dominated by the C = C symmetric stretch.[15,16] Importantly, fitting the individual vibronic peaks of such aggregate-only spectra (using Equation (1), below, for PL or Equation S2, Supporting Information, for absorption) enables us to extract parameters that characterize the material's optoelectronic properties. For instance, from the peak width, we deduce the energetic site disorder, σ . The reason is that the absorption- and PL- peak width is dominated by inhomogeneous broadening caused by a distribution of chromophores that absorb and emit different wavelengths. A narrower absorption/emission peak implies a greater similarity between aggregates and is hence associated with systems in which a larger proportion of aggregates have greater translational and conformational order. From the 0-0/0-1 vibronic peak ratio, the balance between intra- and interchain excitonic coupling is obtained, which can be interpreted in the framework of the weakly interacting H-aggregate model developed by Spano et al.,[4,6,15–18] often applied to P3HT.[5,6,15,16,18] [Note: Normalizing the spectra of non-aggregated areas to the high-energy tail of the overall spectrum implicitly assumes that absorption from aggregates is negligible at higher energies, which is not necessarily the case. For the

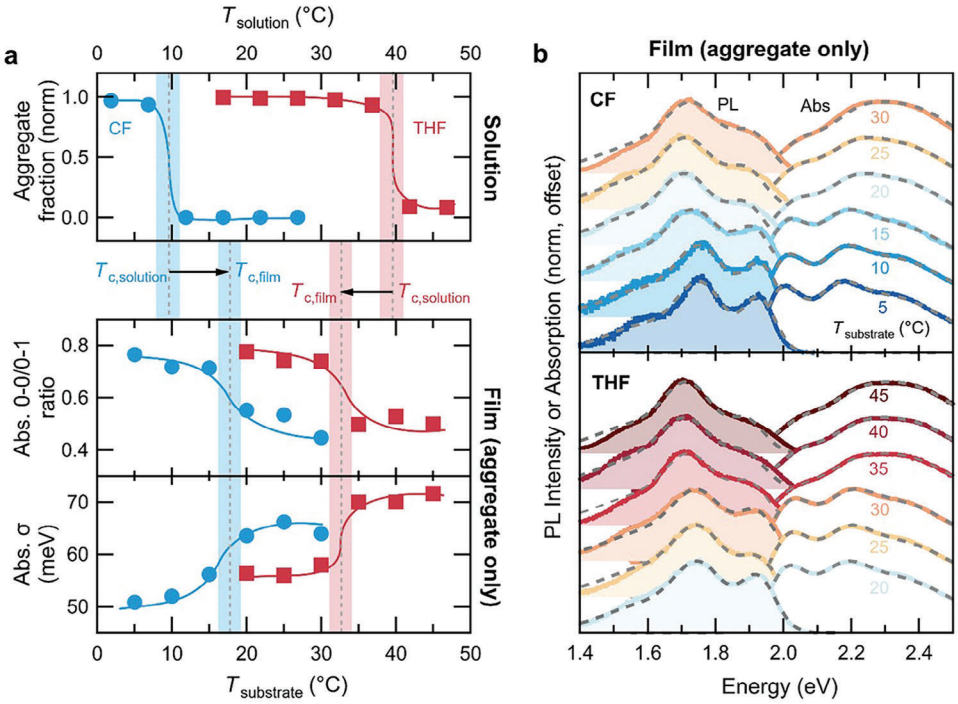

Figure 2. a) Top panel: Solutions. Temperature dependent fraction of aggregated P3HT chains in CF (blue dots) and THF (red squares) solutions. Solid lines guide the eye, with the inflection point (vertical dashed grey lines) corresponding to the critical transition temperature $T_{c,solution}$.. Bottom panel: Films. 0-0/0-1 peak ratio and σ extracted from absorption spectra fits as a function of $T_{substrate}$. The inflection point corresponds to the critical temperature $T_{c,film}$. Notably, this differs from $T_{c,solution}$ for both CF and THF. b) Aggregate-only PL (color shaded) and absorption spectra of P3HT films blade-coated from CF (top) and THF (bottom) solution for different substrate temperatures $T_{substrate}$ (dashed grey lines show best fits using Equation (1) for PL and using Equation S2, Supporting Information, for absorption, details in text).

absorption spectra, this method is associated with some uncertainty in the higher energy spectral range.]

Having a framework to distinguish between non-aggregated and aggregated material allows us to quantify the critical transition temperatures, T_c, below which polymer aggregation occurs, both in (sealed) solutions and during film formation, i.e., upon solvent evaporation.[19] Following the above procedure, we first discuss aggregate formation in sealed CF and THF solutions (10 mg ml^{-1}), respectively. While we observe no absorption features from aggregated chains at elevated temperatures, they appear when the solutions are cooled below, respectively, 12 °C (CF) and 42° (THF), as can be inferred from Figure S1 (Supporting Information). Deducing the fraction of aggregate at different solution temperatures from this data (Figure 2a, top panel), we find sigmoidal dependence, with the point of inflection defining $T_{c,solution}$.

Next, we consider aggregation for films cast at different substrate (i.e., deposition) temperatures, $T_{substrate}$, using solutions in CF and THF also at a 10 mg ml^{-1} concentration. We define $T_{c,film}$ as the maximum deposition (substrate) temperature that leads to pronounced aggregate formation in the resulting, dried films;, i.e., for $T_{substrate} \leq T_{c,film}$, aggregates form readily, while in the case of $T_{substrate} > T_{c,film}$ no, or only very limited, aggregation occurs. Figure 2b shows the PL and absorption aggregate spectra of P3HT films where the non-aggregated component has been subtracted as outlined in Figure 1 (see Figure S2, Supporting Information, for non-decomposed spectra). While all absorption and PL aggregate spectra show the characteristic Franck-Condon vibronic progression associated with P3HT aggregates,[5,15,16] there is a clear dependence of spectral shape on $T_{substrate}$, independent from which solvent (CF vs THF) films were deposited from. For CF, there is little variation in spectral shape between films produced at $T_{substrate} \geq 20$ °C. In comparison, at $T_{substrate} \leq 15$ °C, the 0-0/0-1 vibronic peak ratio increases and the spectra become more structured in both absorption and PL, indicating that higher-quality (i.e., more extended) aggregates only form when using a deposition temperature equal to or below 15 °C. Concomitantly, for $T_{substrate} \geq 20$ °C, both absorption and emission spectra show a significant contribution from non-aggregated chains, while the features from the aggregated chains dominate the spectra for $T_{substrate} \leq 15$°C (Figure S2, Supporting Information). A similar trend can be seen for films coated from THF solutions, although here, the transition in spectral shape occurs between 30 and 35 °C, suggesting that $T_{c,film}$ is notably higher compared to films made from CF.

To quantify the changes of aggregate spectra with substrate temperature and to precisely identify $T_{c,film}$, we fitted the aggregate-only PL spectra using a modified Frack-Condon progression with a decoupled 0-0 peak (with the prefactor α),[15] using the relation:

$$PL(E) \propto E^3 \left[\alpha \exp\left(\frac{(E-E_0)^2}{2\sigma^2} \right) + \sum_{m=1}^{m=3} \frac{S_{eff}^m}{m!} \exp\left(-\frac{(E-(E_0 - mE_{vib}))^2}{2(\sigma + m \cdot \Delta\sigma)^2} \right) \right] \quad (1)$$

where E is energy, E_0 the energetic location of the vibrationless 0-0 peak, m is the peak number, σ is the peak width, and E_{vib} is the effective mode energy, with the Huang-Rhys factor S_{eff} being fixed here to 1.[19] The refractive index is assumed to be constant in the energy range considered here and, therefore, is omitted. Following the approach presented by Yamagata et al.,[20] we included an additional broadening term $m \cdot \Delta\sigma$ in Equation (1). This term accounts for the peak broadening with higher vibronic transitions m due to the overlap of vibronic modes with similar energies,[20] as is the case for P3HT.[21] With this relatively simple modification of the effective-mode Franck–Condon approach, the quality of fits of Equation (1) to the measured PL spectra improves (Figure S3, Supporting Information), ensuring more reliable fitting parameter extraction. [Since the method to extract the aggregate-only absorption spectrum is associated with some uncertainty in the higher energy spectral range of the absorption spectrum, as alluded to above, the reliability of modified Frank Condon analyses of aggregate absorption spectra[6,16] is limited. This is notably less pronounced when fitting the PL spectra. To extract the 0-0/0-1 peak ratio and σ, relevant in this work, it is therefore sufficient to use a more simplified approach for the absorption spectra and to fit Gaussians with equidistant spacing to the aggregate-only spectra (see Figure S3, Supporting Information, for details).]

Figure 2a, bottom panel, shows the 0-0/0-1 peak ratios and the peak widths, σ, extracted from the absorption spectra of films produced at different substrate temperatures (i.e., different deposition temperatures). Both show a sigmoidal dependence with $T_{substrate}$, with a step-like increase in 0-0/0-1 ratio at lower $T_{substrate}$ from ≈0.5 to ≈0.8 observed for films made from either CF and THF, and σ decreasing similarly from 65 to 50 meV for CF and from 70 to 55 meV for THF. Crucially, the inflection points in this sigmoidal behavior yields $T_{c,film}$, the critical transition temperature associated with aggregate formation. We deduce $T_{c,film}$ (CF) ≈ 18 °C and $T_{c,film}$ (THF) ≈ 33 °C, indicated in Figure 2b, bottom panel, with dashed lines. Clearly, the lower solubility of P3HT in THF compared to CF leads to aggregation at higher temperatures during film formation.

It is interesting to compare $T_{c,film}$ and $T_{c,solution}$ (Figure S1, Supporting Information). We find, intriguingly, that $T_{c,solution}$ (CF) ≈ 7 °C, i.e, lower than $T_{c,film}$ (CF). In contrast, $T_{c,solution}$ (THF) ≈ 37 °C is higher than $T_{c,film}$ (THF) (Figure 2a). We suggest that this finding reflects the different interactions in the systems. In a good solvent, such as CF, one can expect solvent-polymer interactions to dominate, preventing aggregation till low temperatures are reached; however, during film casting, where the solvent evaporates, the polymer concentration increases rapidly, leading to aggregate formation at a higher temperature. Vice versa, in a poor solvent, polymer-polymer interactions are already prominent, leading to early aggregation in a sealed solution (that is, aggregation at high temperatures, i.e., high $T_{c,solution}$). If solvent evaporation is allowed, such aggregates can lead to rapid gelation,[22] hindering mass transport and, thereby, limiting aggregate formation, resulting in a $T_{c,sfilm}$ that is lower than $T_{c,solution}$. Accordingly, simple criteria can be set for solvent selection which can be anticipated to become a useful tool to understand less studied polymer/solvent combinations.

In order to test this view and gain further insights into the difference between polymer aggregation in a good versus a poor solvent, we continued to record the temporal evolution of the optical properties of the P3HT wet layers throughout the film formation process. For this purpose, we performed concurrent in situ absorption and PL measurements during blade coating of P3HT solutions at different substrate temperatures (see the Experimental Section in Supporting Information for details).[23] We start by discussing P3HT solutions in CF, cast at $T_{substrate}$ = 5 °C (i.e., << $T_{c,films}$) and $T_{substrate}$ = 25 °C (i.e., >> $T_{c,film}$). **Figure 3** shows the absorption spectra along the corresponding PL spectra taken at different times during blade coating, with t = 0 s referring to the onset of the blade-coating (the moment the glass blade moves over the local area where we record the spectra; see Experimental Section for details).

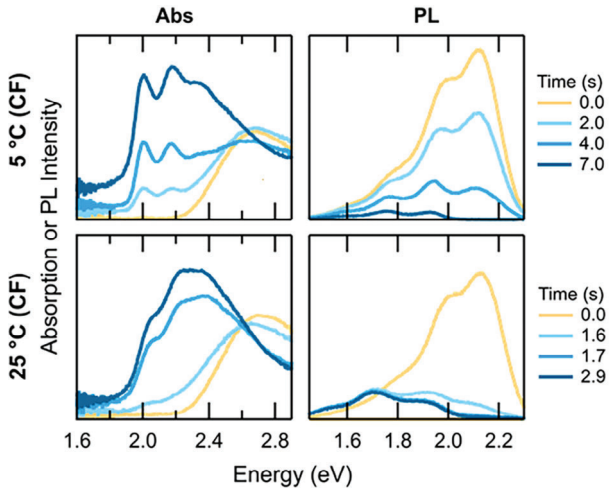

Figure 3. Absorption (left) and PL (right) spectra as measured in situ during blade coating P3HT in CF at $T_{substrate}$ = 5 °C (top) and 25 °C (bottom).

We observe a clear transition in the spectral line shapes during film drying at both substrate temperatures. Broad spectral features dominate the initial spectra at early times of the coating process at ≈2.7 eV in absorption and ≈2.1 eV in PL. These are characteristic of non-aggregated P3HT. At later times, the casting temperatures have a substantial impact. When using $T_{substrate}$ = 5°C, the spectra show features that indicate aggregate formation, including well-resolved and intense 0-0 peaks observed at lower energies (2.0 eV in absorption and 1.9 eV in PL), leading to a clear vibronic structure and a high 0-0/0-1 intensity ratio. In comparison, for $T_{substrate}$ = 25 °C, the vibronic structure is less pronounced and a relatively low 0-0/0-1 intensity ratio is recorded.

More details are obtained from time-resolved, aggregate-only absorption and PL spectral maps, provided in **Figure 4**, top panel, for films produced from CF, cast at 5 and 25 °C. Also shown are the normalized intensities, calculated from peak integrals of the aggregate-only spectra and indicative of the aggregate fraction within the wet layer/dried film; the 0-0/0-1 ratio; as well as the Gaussian peak width, σ, determined by fitting Equation (1) and Equation S2 (Supporting Information) (see Figures S4,S5 (Supporting Information) for exemplary fits and residuals for films cast at $T_{substrate}$ = 5 °C) and providing information on the degree of aggregate disorder (Figure 4, bottom panel).

At $T_{substrate}$ = 5 °C, i.e., at $T_{substrate}$ << $T_{c,film}$, absorption and emission signatures for aggregated chains are observed starting

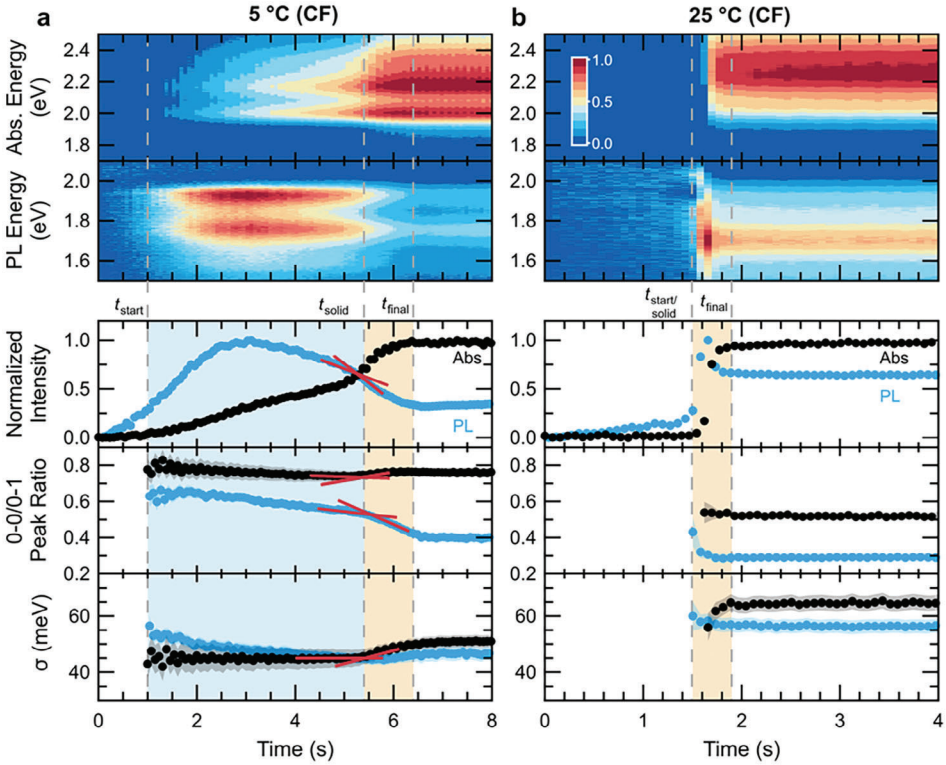

Figure 4. Evolution of absorption and PL spectra during blade coating P3HT from CF solution at $T_{substrate}$ = 5 °C (a) and 25 °C (b). Top panels show 2D heat maps of aggregate-only absorption and PL spectra. Bottom panels show the normalized intensity, 0-0/0-1 peak ratio and σ extracted from absorption (black) and PL (blue) spectra. Characteristic times are assigned when the normalized absorption intensity of the aggregates exceeds 3% (t_{start}) of the final film value, when there is a kink in the evolution of optical parameters (t_{solid}), and when the absorption normalized intensity (i.e., aggregate fraction) reaches unity (t_{final}). Colored shading indicates periods between these characteristic times. Red tangents in (a), bottom panels, assist in identifying t_{final}.

at $t \approx 1.0$ s (Figure 4a, top panel). Thereby, the aggregate absorption intensity increases continuously till $t \approx 6.4$ s. In parallel, the aggregate PL intensity rises to a maximum after only 3.0 s, after which it decreases before levelling off ≈6.4 s. We attribute this to the greater photoluminescence quantum yield (PLQY) of the polymer aggregates that form within the solution at this $T_{substrate}$, where intra-aggregate interactions and hence photoluminescence quenching are reduced. This interpretation is supported by the PL intensity reaching a maximum midway through the initial aggregation phase (from t_{start} to t_{solid}) for the 5 °C sample—which we infer to be a sweet spot in aggregate concentration that maximizes the number of emissive aggregates but minimizes inter-aggregate interactions.

When blade-coating well above $T_{c,film}$ ($T_{substrate}$ = 25 °C; Figure 4b, top panel), aggregate PL sets in at a later stage (after 1.5 s), with a very sharp, rapid increase in the aggregate absorption intensity that saturates around $t \approx 1.9$ s. We note that for both temperatures, some PL from the aggregates can be identified before characteristic features appear in the absorption spectra (i.e., before 1.0 s at 5 °C and before 1.5 s at 25 °C). We interpret this as an indication of excimer-like pre-aggregation features, i.e., chromophores that can interact in the (usually more planar) excited state geometry while no such interaction occurs in the ground state geometry.

The above observations allow us to identify characteristic times within the solidification process, using information on the time evolution of the normalized intensities, 0-0/0-1 peak ratios, and σ (Figure 4, bottom panels). For this purpose, we define the onset of aggregate formation t_{start}, as the time when the spectrally integrated aggregate absorbance exceeds 3% of its maximum value; the time at which all three parameters display a distinct change in their dependence with time (observed as a change in slope, indicated with red tangents in Figure 4a, bottom panels), we assign to the moment when most solvent is evaporated (i.e., t_{solid});[19] and, the time where no further changes to the aggregate spectra occur within a 5% experimental error range is t_{final}. Accordingly, at $T_{substrate}$ = 5°C, $t_{start} \approx 1.0$ s, t_{solid} ≈5.4 s, and $t_{final} \approx 6.4$ s (Figure 4a, bottom panel). From this, we conclude that aggregation occurs via a two-step process; at t_{start}, aggregates begin forming in solution until t_{solid} is reached (light blue shaded area). Since this is a scenario where the polymer chains evidently must have high molecular mobility and high mass transport, provided by the solvent-rich environment, aggregates are induced that are of relatively low torsional disorder (low σ) and lead to comparatively strong intra-molecular excitonic coupling (high 0-0/0-1 peak ratio). From t_{solid} to t_{final} (pale orange region), these aggregates undergo some disordering, as deduced from the slight increase in σ and the reduced 0-0/0-1 peak ratio, especially in PL, indicative of a reduced intra-chain excitonic coupling.

This picture changes when casting above $T_{c,film}$, at $T_{substrate}$ = 25°C (Figure 4b, bottom panel). Here, solidification occurs via a one-step process, with the onset of aggregation essentially

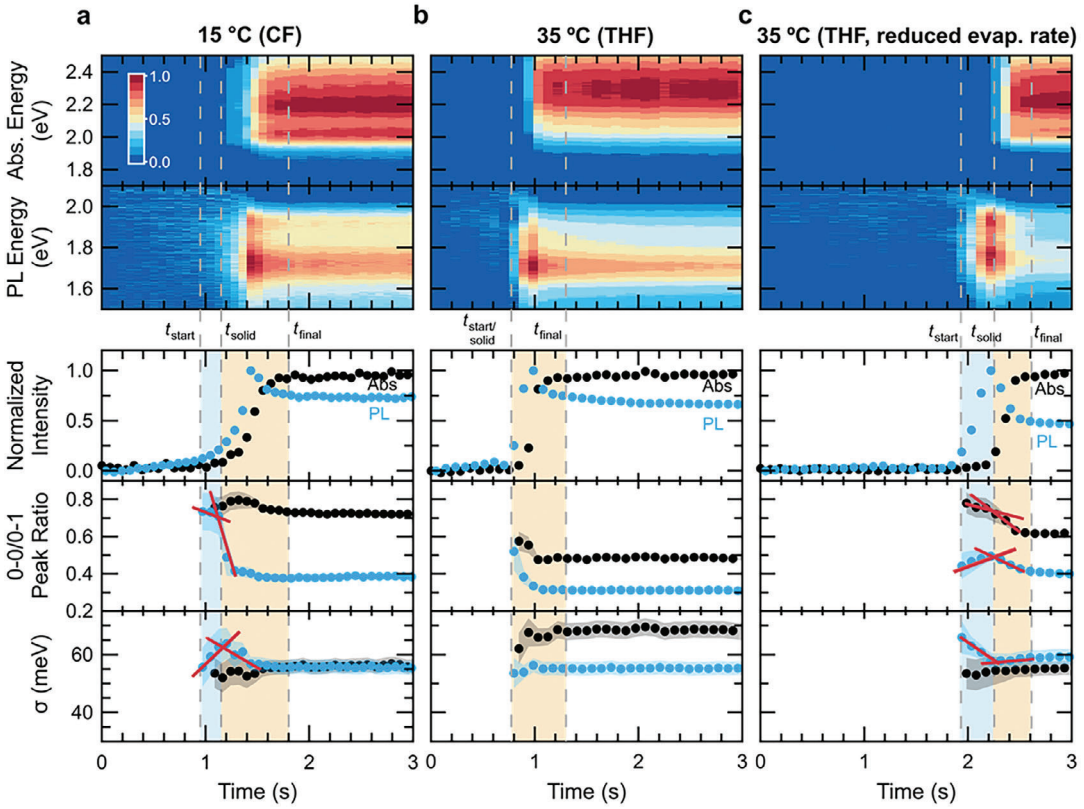

Figure 5. Evolution of absorption and PL spectra during blade coating P3HT from CF at $T_{substrate}$ = 15 °C (a), from THF at $T_{substrate}$ = 35 °C (b), and THF at $T_{substrate}$ = 35 °C with a reduced evaporation rate (c). Top panels show 2D heat maps of aggregate-only absorption and PL spectra. Bottom panels show the normalized intensity, 0-0/0-1 peak ratio and σ extracted from absorption (black) and PL (blue) spectra. Characteristic times are assigned similarly to Figure 4. Red tangents in (a,c), bottom panels, assist in identifying t_{final}.

coinciding with complete solvent evaporation (i.e., $t_{start} \approx t_{solid} \approx$ 1.5 s) and rapidly reaching saturation of aggregate formation at t_{final} = 1.9 s. This means that, when using $T_{substrate} > T_{c,film}$, no solution aggregation occurs; instead, aggregation occurs within 0.4 s when an environment that is highly enriched in polymer is reached, leading to vitrification due to drastic decreases in mass transport and molecular mobility. This leads to aggregates of low torsional order and high energetic site disorder (high σ) and, in turn, to a comparatively low intra-chain excitonic coupling (low 0-0/0-1 peak ratio).[5,6,19,24]

Holistically, our results imply that by knowing $T_{c,film}$ and $T_{substrate}$, the aggregate formation mechanism of polymer semiconductors processed from solution can be manipulated. This view is supported by the observations made on films produced from THF, which behave rather similar to films deposited from CF (Figure S6, Supporting Information). Casting at $T_{substrate} < T_{c,film}$, including 20, 25, and 30 °C, clear aggregate formation in solution is recorded, while aggregates develop in a 1-step process when using substrate temperatures of 35, 40, and 45 °C (i.e., $T_{substrate} > T_{c,film}$). Most importantly, even better control can be achieved considering also $T_{c,solution}$. Indeed, we can use knowledge of $T_{c,solution}$ to seed aggregates. For instance, if P3HT solutions in CF are cast at 15 °C where $T_{c,solution} < T_{substrate} < T_{c,film}$, solution aggregation is limited, but aggregate seeds are formed because the solution is just above $T_{c,solution}$. Consequently, aggregation essentially follows a 1-step process, with a minimal and short solution aggregation step but, nevertheless, capable of inducing high-quality aggregates (**Figure 5a**, compare also to Figure 2a for the spectra). Unambiguously, using longer seeding procedures, e.g., in a sealed solution prior to casting, or use of higher-boiling-temperature solvents, should assist in further increasing aggregate order and, hence, improving the electronic coupling between chromophores. Seeding also helps to minimize vitrification when processing from a poor solvent such as THF. Relatively well-pronounced aggregation can be obtained provided the assembly kinetics are carefully controlled. For instance, at $T_{substrate}$ = 35°C where $T_{c,film} < T_{substrate} < T_{c,solution}$, the evaporation rate has to be limited to allow seeding to take place. This is shown in Figure 5b,c. If solvent is permitted to evaporate unhindered, a typical 1-step process dominated by solidification-induced aggregation occurs, leading to poorly defined aggregates (high σ, low 0-0/0-1 peak ratio; Figure 5b, bottom panel). Yet, if the films are cast in a solvent-rich environment limiting the solvent evaporation, a short solution-aggregation step is induced through seeding, resulting in aggregates of relatively high torsional order and, better electronic coupling (higher 0-0/0-1 peak ratios).

3. Conclusion

Similar to the solidification of bulk commodity polymers or small molecular semiconductors, the selection of the casting temperature (determined by $T_{substrate}$) based on thermodynamic ($T_{c,solution}$)

and kinetic considerations (reflected by $T_{c,film}$) allows establishing rather precise guidelines for polymer aggregate formation, independent whether a good or a poor solvent is used. Since our criteria can be selected based on the knowledge of $T_{c,solution}$ and $T_{c,film}$, we expect our "recipes" to be broadly applicable. This will be particularly important for the next generation of polymer semiconductors, where the phase behavior is dictated by the backbone assembly and often complex side-chain substituents. Adaption of our approach and findings to these more complex polymers, including donor-acceptor materials used in photovoltaic devices[12,25,26] and doped macromolecules,[27] can be expected to be straight-forward because various studies have already applied spectroscopic probing of aggregate structure to them, with promising results. Overall, our work promises reduced trial and error. Indeed, with a few relatively straight-forward in situ measurements of optical parameters in sealed solutions as well as drying films, clear and very precise casting conditions can be selected, promising faster materials discovery and accelerated and more robust processing of a broad range of devices, including thin-film transistors, diodes, photodetectors, sensors, and with impact on the broader organic energy harvesting and energy storage field.

Supporting Information

Supporting Information is available from the Wiley Online Library or from the author.

Acknowledgements

M.D., H.B., M.C., N.S., and A.K. thank the Marie Sklodowska-Curie Actions Innovative Training Network 'H2020- MSCA-ITN-2014 INFORM—675867' for funding; and M.D., P.S., and N.S. acknowledge the UK Engineering and Physical Sciences Research Council (EPSRC) for funding via the Centre for Doctoral Training in Plastic Electronics Materials (EP/G037515/1). M.D. is grateful to the Royal Society of Chemistry (RSC) for a Researcher Mobility Grant along with Sebastian Engmann and Lee Richter for instructive scientific discussions. N.S. in addition appreciates support by the U.S. National Science Foundation (CHEM #2108123), and assistance of Henry Kantrow at Georgia Tech for measurement of P3HT visoscities.

Conflict of Interest

The authors declare no conflict of interest.

Author Contributions

F.P. and M.J.D. contributed equally to this work. F.P. led the study, performed the analysis and data interpretation and the arrangements of the figures. The solution measurements and analysis were carried out by K.S.. The film measurements and analysis were performed by M.J.D., H.B., M.C., and S.W.. The manuscript was written by M.J.D., F.P., S.W., A.K., and N.S.; all authors reviewed the finished manuscript. P.N.S., N.S., and A.K. supervised work in their respective groups. A.K. and N.S. finalized the manuscript and advanced the overall conclusions of the work.

Data Availability Statement

The data that support the findings of this study are available from the corresponding author upon reasonable request.

Keywords

aggregate formation, printed electronics, semiconducting polymers

Received: November 21, 2023
Revised: January 19, 2024
Published online: February 13, 2024

[1] N. D. Treat, P. Westacott, N. Stingelin, *Annu. Rev. Mater. Res.* **2015**, *45*, 459.
[2] a) F. P. V. Koch, J. Rivnay, S. Foster, C. Müller, J. M. Downing, E. Buchaca-Domingo, P. Westacott, L. Y. Yu, M. J. Yuan, M. Baklar, Z. P. Fei, C. Luscombe, M. A. McLachlan, M. Heeney, G. Rumbles, C. Silva, A. Salleo, J. Nelson, P. Smith, N. Stingelin, *Prog. Polym. Sci.* **2013**, *38*, 1978. b) R. Noriega, J. Rivnay, K. Vandewal, F. P. V. Koch, N. Stingelin, P. Smith, M. F. Toney, A. Salleo, *Nat. Mater.* **2013**, *12*, 1038; c) O. G. Reid, J. A. Nekuda Malik, G. Latini, S. Dayal, N. Kopidakis, C. Silva, N. Stingelin, G. Rumbles, *J. Pol. Phys. B: Pol. Phys.* **2012**, *50*, 27.
[3] I. Botiz, S. Astilean, N. Stingelin, *Polym. Int.* **2016**, *65*, 157.
[4] N. J. Hestand, F. C. Spano, *Chem. Rev.* **2018**, *118*, 7069.
[5] F. Panzer, H. Bässler, A. Köhler, *J. Phys. Chem. Lett.* **2017**, *8*, 114.
[6] F. C. Spano, C. Silva, *Annu. Rev. Phys. Chem.* **2014**, *65*, 477.
[7] a) S. Han, X. Yu, W. Shi, X. Zhuang, J. Yu, *Organic Electron.* **2015**, *27*, 160; b) A. Kumar, M. A. Baklar, K. Scott, T. Kreouzis, N. Stingelin-Stutzmann, *Adv. Mater.* **2009**, *21*, 4447.
[8] A. Köhler, H. Bässler, Electronic Processes in Organic Semiconductors: An Introduction, Wiley-VCH Verla GmbH & Co. **2015**.
[9] F. Paquin, H. Yamagata, N. J. Hestand, M. Sakowicz, N. Bérubé, M. Côté, L. X. Reynolds, S. A. Haque, N. Stingelin, F. C. Spano, C. Silva, *Phys. Rev. B* **2013**, *88*, 155202.
[10] F. Paquin, G. Latini, M. Sakowicz, P. L. Karsenti, L. Wang, D. Beljonne, N. Stingelin, C. Silva, *Phys. Rev. Lett.* **2011**, *106*, 197401.
[11] a) L. J. Richter, D. M. DeLongchamp, F. A. Bokel, S. Engmann, K. W. Chou, A. Amassian, E. Schaible, A. Hexemer, *Adv. Energy Mater.* **2015**, *5*, 1400975; b) L. J. Richter, D. M. DeLongchamp, A. Amassian, *Chem. Rev.* **2017**, *117*, 6332; c) R. Hildner, A. Köhler, P. Müller-Buschbaum, F. Panzer, M. Thelakkat, *Adv. Energy Mater.* **2017**, *7*, 1700314.
[12] K. Zhao, H. U. Khan, R. Li, Y. Su, A. Amassian, *Adv. Funct. Mater.* **2013**, *23*, 6024.
[13] a) C. M. Hansen, *Hansen Solubility Parameters: A User's Handbook, Second Edition*, CRC Press, Boca Raton, FL, USA **2007**; b) D. T. Duong, B. Walker, J. Lin, C. Kim, J. Love, B. Purushothaman, J. E. Anthony, T. Q. Nguyen, *J. Polym. Sci. Pol. Phys.* **2012**, *50*, 1405.
[14] a) P. Grégoire, E. Vella, M. Dyson, C. M. Bazán, R. Leonelli, N. Stingelin, P. N. Stavrinou, E. R. Bittner, C. Silva, *Phys. Rev. B* **2017**, *95*, 180201; b) O. J. Korovyanko, R. Österbacka, X. M. Jiang, Z. V. Vardeny, R. A. J. Janssen, *Phys. Rev. B* **2001**, *64*, 235122.
[15] J. Clark, C. Silva, R. H. Friend, F. C. Spano, *Phys. Rev. Lett.* **2007**, *98*, 206406.
[16] J. Clark, J. F. Chang, F. C. Spano, R. H. Friend, C. Silva, *Appl. Phys. Lett.* **2009**, *94*, 163306.
[17] a) H. Yamagata, F. C. Spano, *J. Chem. Phys.* **2012**, *136*, 184901; b) F. C. Spano, *J. Chem. Phys.* **2005**, *122*, 234701.
[18] F. C. Spano, J. Clark, C. Silva, R. H. Friend, *J. Chem. Phys.* **2009**, *130*, 074904.
[19] M. Reichenberger, D. Kroh, G. M. M. Matrone, K. Schötz, S. Pröller, O. Filonik, M. E. Thordardottir, E. M. Herzig, H. Bässler, N. Stingelin, A. Köhler, *J. Polym. Sci., Part B: Polym. Phys.* **2018**, *56*, 532.
[20] H. Yamagata, D. S. Maxwell, J. Fan, K. R. Kittilstved, A. L. Briseno, M. D. Barnes, F. C. Spano, *J. Phys. Chem. C* **2014**, *118*, 28842.

[21] a) C. Scharsich, F. S. U. Fischer, K. Wilma, R. Hildner, S. Ludwigs, A. Köhler, *J. Polym. Sci. Pol. Phys.* **2015**, *53*, 1416; b) S. Garreau, M. Leclerc, N. Errien, G. Louarn, *Macromolecules* **2003**, *36*, 692; c) L. Farouil, F. Alary, E. Bedel-Pereira, J. L. Heully, *J. Phys. Chem. A* **2018**, *122*, 6532; d) M. Ariu, D. G. Lidzey, M. Lavrentiev, D. D. C. Bradley, M. Jandke, P. Strohriegl, *Synthetic Met.* **2001**, *116*, 217; e) J. J. Sutton, T. L. Nguyen, H. Y. Woo, K. C. Gordon, *Chem.-Asian J.* **2019**, *14*, 1175; f) J. Gao, J. Wang, Q. An, X. Ma, Z. Hu, C. Xu, X. Zhang, F. Zhang, *Sci. China: Chem.* **2020**, *63*, 83.

[22] Z. X. Peng, N. Stingelin, H. Ade, J. J. Michels, *Nat. Rev. Mater.* **2023**, *8*, 439.

[23] M. Buchhorn, S. Wedler, F. Panzer, *J. Phys. Chem. A* **2018**, *122*, 9115.

[24] C. Scharsich, R. H. Lohwasser, M. Sommer, U. Asawapirom, U. Scherf, M. Thelakkat, D. Neher, A. Köhler, *J. Polym. Sci. Pol. Phys.* **2012**, *50*, 442.

[25] H. Ma, Z. Sun, M. Jeong, S. Yang, S. Jeong, S. Lee, Y. Cho, J. Park, J. Park, C. Yang, *Chem. Eng. J.* **2023**, *474*, 145531.

[26] Y. Q. Zheng, Z. F. Yao, T. Lei, J. H. Dou, C.-Y. Yang, L. Zou, X. Meng, W. Ma, J. Y. Wang, J. Pei, *Adv. Mater.* **2017**, *29*, 1701072.

[27] M. Xiong, X. Yan, J. T. Li, S. Zhang, Z. Cao, N. Prine, Y. Lu, J.-Y. Wang, X. Gu, T. Lei, *Angew. Chem., Int. Ed.* **2021**, *60*, 8189.